Korean J. Chem. Eng., 34(2), 287-297 (2017)
DOI: 10.1007/s11814-016-0292-2

pISSN: 0256-1115
eISSN: 1975-7220

Dynamic matrix control applied on propane-mixed refrigerant liquefaction process

Hyunjun Shin*,‡, Yu Kyung Lim,‡, Se-Kyu Oh**, Seok Goo Lee**, and Jong Min Lee**,†**

*Daewoo Shipbuilding & Marine Engineering Co., Ltd., 125 Namdaemun-ro, Jung-gu, Seoul 04521, Korea
**School of Chemical & Biological Engineering, Institute of Chemical Processes,
Seoul National University, 1 Gwanak-ro, Gwanak-gu, Seoul 08826, Korea
(*Received 22 June 2016 • accepted 15 October 2016*)

Abstract−This study proposes a dynamic matrix control strategy that produces control input sequences which are more robust and reduce power consumption than conventional proportional-integral (PI) controllers when applied to the C3MR liquefaction process. First, a rigorous process dynamic model was constructed in Aspen HYSYS Dynamics 7.3 and MATLAB 2014a which calculates dynamic responses for two different scenarios of unmeasured step disturbances increasing the load of liquefaction energy. Then, a DMC module including the manipulation of the compressor speed was formulated. The simulations using the proposed DMC module demonstrate that the multivariable optimal control increases the energy efficiency and robustness of a complex liquefaction cycle process.

Keywords: LNG Liquefaction, C3MR Process, DMC, APC, Cascade PI Control

INTRODUCTION

While the use of the crude oil is mostly concentrated in the transportation sector, natural gas (NG) can be utilized more widely, its usage covering not only the power generation but also the industrial and residential sectors. Such flexibility, higher BTUs generated per dollar than crude oil, less emission of greenhouse gas and polluting oxidants and significantly lower price volatility since the dawn of the shale gas boom at 2009 [1-4] make NG still an attractive energy source, despite the current price plunge of the crude oil [5]. NG occupied 22% of the global energy demand in 2010; this percentage is expected to rise to 27% by 2040, including an estimated 15% increase in the heavy transportation sector in China and India [6,7]. Such expansion of the NG market encourages further developments of the liquefied natural gas (LNG) production and transportation industries.

NG is processed into LNG to increase the transport efficiency by decreasing its physical volume. The propane pre-cooled mixed refrigerant (C3MR) process developed by Air Products, Inc. has become dominant in the NG liquefaction industry since the late 1970s [8]. At the current stage, the operation and control methods of the C3MR process are already fairly standardized with the proportional-integral-derivative (PID) control algorithm. However, there is still a significant possibility that the industry could call for further optimization of the C3MR process as the developments of new off-shore site gas liquefaction projects such as the floating liquefied natural gas (FLNGs) are gaining attention, with the LNG demand being expected to rise in long-term [9-13]. If a traditional liquefaction process goes aboard on off-shore carriers such as an FLNG, it will be under process constraints that are generally stricter than those of the on-shore applications. They include not only higher energy efficiency, a more compact structure and process safety [12, 14], but also robustness against process disturbances. Especially the latter should be more strongly guaranteed in comparison with the on-shore equivalents [13,14], since the metocean conditions may impose various situations causing FLNGs shift away frequently from the steady-state operation [9].

Considering such current interest regarding the NG liquefaction industry, we aim to demonstrate that advanced process control (APC) can be successfully applied to the C3MR process and handle unmeasured process disturbances with more robustness. Dynamic matrix control (DMC), which is a branch of the model predictive control (MPC) algorithm, is a frequently used APC technique applied to large-scale process plants [15-17]. It is a multivariable controller that predicts the future behavior of the process outputs with the moving-horizon control algorithm and achieves more efficient disturbance rejection and constraint satisfaction than the PID controllers, especially if there are significant multivariable interactions present within the process [4,18-21]. The use of DMC algorithm on LNG plants has significantly expanded in last decade, including some of the widely known projects such as the Oman LNG-train (U1400) and the APC project based on the Shell DMR process. The efficiency of these projects has improved, resulting in 1-3% higher LNG throughput and stronger stability against process disturbances [4,22]. Also, several recommended sets of controlled variables (CV), manipulated variables (MV) and measured disturbances for the DMC application for a liquefaction process were mentioned in a special report [18]. To our knowledge however, a rigorous research about the application of the DMC method on the C3MR process needs yet to be proposed.

The necessity of applying the multivariable optimal control on the C3MR process was brought up in a previous study in which a process simulation result is validated by the experimental data sug-

†To whom correspondence should be addressed.
E-mail: jongmin@snu.ac.kr
‡First co-authors.

gesting that multiple MVs such as the flow rates of both phases of cooling mixed-refrigerant (CMR) and the flow rate of LNG stream interact with multiple CVs, including the CMR temperatures at different locations of heat exchangers. Hence, rather than a single-loop control, a cascade control strategy or an MPC method was suggested as a possible breakthrough that may enhance the process efficiency [23]. Since the cascade feedback control is already included in commercial LNG liquefaction processes [24], we demonstrate a case study in which a two-by-three structured DMC module regulates the CMR loop inside the C3MR process against two different scenarios of unmeasured process disturbances. The process example and the control structure are based on a research of the optimal configuration of the single-input-single-output (SISO) controllers on the C3MR process [25]. Our purpose is to compare the DMC simulation result with the results of a two-by-two and three-by-three structured cascade PI controllers run against the same scenarios. A rigorous process model of the C3MR process is built on the Aspen HYSYS 7.3, which is either regulated by the PI controllers on the same process simulator environment or by the DMC method built on the MATLAB 2014a. The DMC is formulated using a step response coefficient matrix obtained by the system identification of the dynamic process model on the Aspen HYSYS 7.3. The improving robustness of the MV sequences and their effect on the process power consumption are discussed in the concluding remarks.

DYNAMIC SIMULATION OF THE C3MR PROCESS

1. Process Description

A detailed explanation of the C3MR process illustrated in Fig. 1 and the operational conditions of the main process units are provided in this section. The C3MR process is comprised of two separate cooling cycles: the C3 cooling cycle that includes the pre-cooler and the CMR cooling cycle with the main cryogenic heat exchanger (MCHE) having a liquefier and a subcooler subunits [25].

After the pre-treatment process, the NG feed is cooled from 30 °C to −40 ~ −30 °C by passing through the pre-cooler. The feed is further cooled by the MCHE module, expanded by the LNG V/V valve and reaches the final product temperature of −159 °C. The C3 cycle shares the duty of the CMR cycle and cools both the NG and CMR prior to the MCHE [26]. mainly illustrates the CMR cycle as the C3 cycle is out of the scope of this study and thus the C3 cycle is shown as a simplified single pre-cooler module coming after the compressor cycle. The average molecular weight of the CMR is usually lower than C3 because the MCHE must achieve stronger cooling power than the pre-cooler. The general composition of the CMR is 90% of methane (C1), ethane (C2) and C3. The remaining 10% consists of nitrogen (N2) and occasionally n-butane (n-C4) [26,27]. After the CMR stream absorbs heat from the NG stream, it is condensed and liquefied again by going through the CMR compressor module and the pre-cooler. The CMR compressor module is a two-stage rotary screw type compressor unit. The compressors are connected by a single axis that rotates their impellers at the same RPM speed. After the CMR is compressed from 3-5 barA to 40-60 barA by the compressors, it becomes a two-phase (vapor-liquid) stream when it is cooled to −40 ~ −30 °C by passing through the pre-cooler. The CMR vapor (CMRV) and the liquid (CMRL) are separated before entering the MCHE. These CMRV and CMRL streams handle the major duty loads coming from the liquefier and the subcooler by utilizing the temperature decrease resulting from the Joule-Thomson (JT) expansion. We assume for the plate fin heat exchanger model of the MCHE that a layer pattern module is stacked repeatedly inside the heat exchangers. The stream layer pattern configurations of the liquefier and the subcooler are DCDBDAD repeated 238 times and EAEBEAE repeated 20 times, respectively, where A: NG, B: CMRL, C: CMRV, D: CMR cold stream, and E: CMRV cold stream.

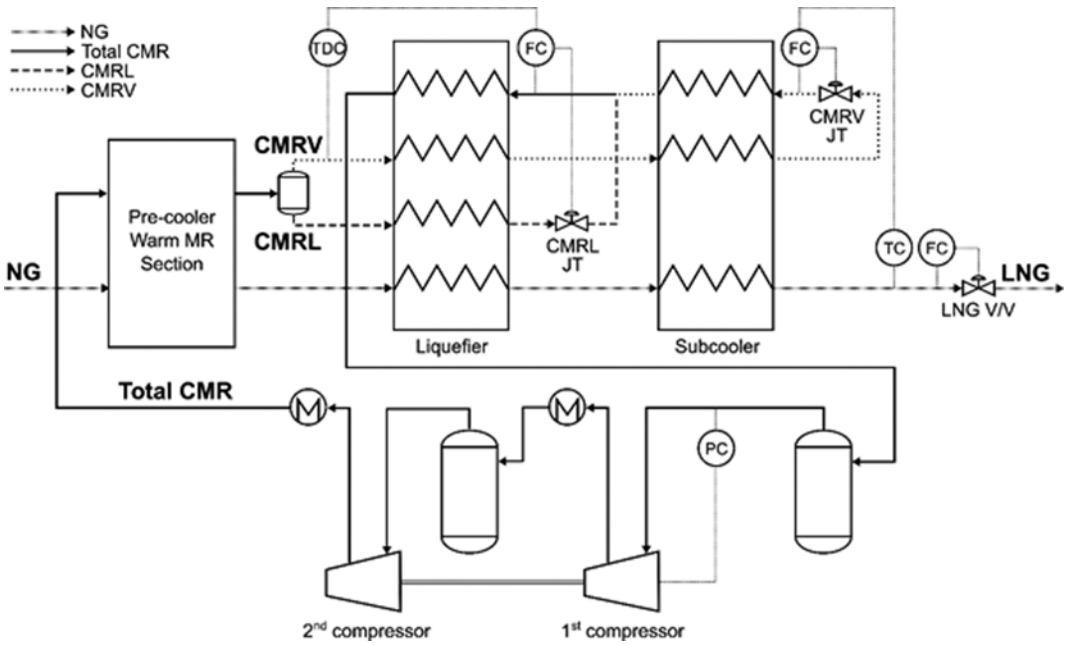

Fig. 1. Overall scheme of the C3MR process.

2. Process Simulation

Two separate property methods are selected for the process simulation of a high-pressure nonpolar hydrocarbon system. First, the Peng-Robinson equation in Eq. (1) is employed as the main equation of state (EOS) of the Aspen HYSYS simulation, where descriptions of the additional accompanying parameters are found in [28,29]. This EOS provides accurate results of the vapor-liquid equilibrium (VLE) calculations for a hydrocarbon mixture system over a wide range of operation conditions.

$$P = \frac{RT}{V_m - b} - \frac{a(T)}{V_m(V_m + b) + b(V_m - b)} \tag{1}$$

In addition, the Lee-Kesler method is specified as the calculation method for the enthalpy and the entropy deviation since it provides an accurate enthalpy model for nonpolar gas mixtures [30]. This method utilizes the compressibility factor Z that is obtained by the Pitzer's correlation in Eq. (2), where Z^r and Z^0 are calculated by the Benedict-Webb-Rubin (BWR) EOS in Eq. (3).

$$Z = Z^0 + \frac{\omega}{\omega^r}(Z^r - Z^0) \tag{2}$$

$$Z = 1 + \frac{B}{V_r} + \frac{C}{V_r^2} + \frac{D}{V_r^5} + \frac{c_4}{T_r^3 V_r^2}\left(\beta + \frac{\gamma}{V_r^2}\right)\exp\left(-\frac{\gamma}{V_r^2}\right) \tag{3}$$

$$V_r = \frac{V_m P_c}{RT_c} \tag{4}$$

where T_r, P_r, V_r^0, Z^0 and Z^r are calculated at the specified temperature T and the pressure P, the deviations of the enthalpy H and the entropy S from the ideal state are computed by Eqs. (4)-(5). Further detailed calculation procedures of these departure functions are illustrated in various references including [31,32].

$$\left(\frac{H^0 - H}{RT_c}\right) = \left(\frac{H - H^0}{RT_c}\right)^0 + \frac{\omega}{\omega^r}\left[\left(\frac{H^0 - H}{RT_c}\right)^r - \left(\frac{H^0 - H}{RT_c}\right)^0\right]$$
$$\left(\frac{S^0 - S}{R}\right) = \left(\frac{S - S^0}{R}\right)^0 + \frac{\omega}{\omega^r}\left[\left(\frac{S^0 - S}{R}\right)^r - \left(\frac{S^0 - S}{R}\right)^0\right] \tag{4}$$

$$\left(\frac{H^0 - H}{RT_c}\right)^0 = f_1(T_r, V_r^0, Z^0, b_2, b_3, b_4, c_2, c_3, d_2, E)$$
$$\left(\frac{S^0 - S}{R}\right)^0 = f_2(T_r, V_r^0, Z^0, b_1, b_3, b_4, c_1, c_3, d_1, E) \tag{5}$$

The process flow diagram (PFD) in Aspen HYSYS environment shown in Fig. 2 is used for both the steady-state and the subsequent dynamic simulations with a time step of Δt=0.5 s and the actuator travel time of the control valves being 5 s/%. The operational conditions of both NG feed and CMR stream used in both simulations are shown in Table 1.

Initially, a steady-state process simulation is conducted using the boundary condition of the NG feed and the CMR stream shown in Table 1. The operating parameters used in this simulation are summarized in Table 2. The steady-state solution then acts as the initial condition of the subsequent dynamic simulations. Additional information about the compressor performances is provided in the Appendix.

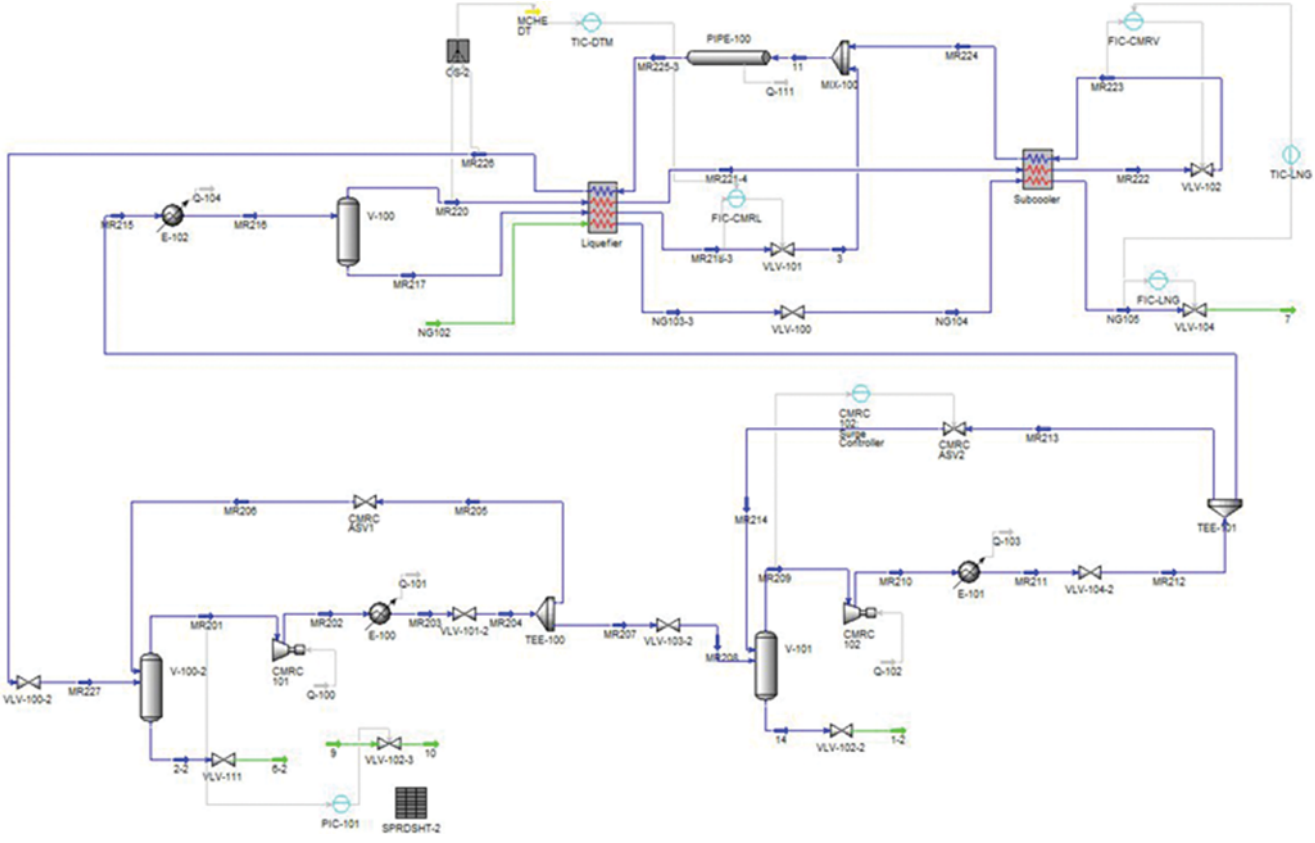

Fig. 2. PFD of the C3MR process built in Aspen HYSYS dynamics 7.3.

Table 1. Operation condition of the NG feed and the CMR stream at steady-state

NG feed	
Description [Unit]	Value
Mass flow rate [ton/h]	214.7
Inlet pressure [barA]	65
Outlet pressure [barA]	1.25
Inlet temperature [°C]	30
Outlet temperature [°C]	−159.1
Pressure after pre-cooler [barA]	58.79
Temperature after pre-cooler [°C]	−33.15
CMR stream	
Description [Unit]	Value
Mass flow rate [ton/h]	482
CMRV flow rate [ton/h]	135.2
CMRL flow rate [ton/h]	346.8
Suction pressure of the 1st compressor [barA]	4.03
Discharge pressure [barA]	51.82
Suction temperature [°C]	−38.87
Discharge temperature [°C]	29.96
Pressure after pre-cooler [barA]	49.07
Temperature after pre-cooler [°C]	−32.82
Temperature difference of liquefier [°C]	5.86

CONTROLLER FORMULATION

1. Control Structure Configuration

A multi-input-multi-output (MIMO) control structure of the DMC controller is chosen using the MVs and CVs suggested in a reference study. The validity of this multivariable control structure is supported by studying the interactions between the process variables which are obtained through the steady-state relative gain array (RGA) analysis. The control performance of the proposed DMC control structure is then compared with the counter-examples of two different cascade PI controllers.

In the first step, the control structures available in the C3MR process need to be configured. We refer to a previous research that identified the available SISO feedback control structures of the same process [25] by following the rule of counting the actual degree of freedom (DOF) [33]. There are initially total 9 available MVs in the C3MR process which are mentioned in the following list:

- CMRL flow rate (CMRL JT valve) (1), CMRV flow rate (CMRV JT valve) (2)
- LNG flow rate (LNG V/V) (3)
- CMR compressor speed (4)
- Pre-cooler refrigerant flow rate (Pre-cooler refrigerant JT valve) (5)
- Cooling medium flow rates for the CMR compressor intercooler (6) and the aftercooler (7)
- CMR anti-surge valves (8, 9)

The equipment name in the parentheses is the actuator valve related to each MV. It is desirable if the dynamic model structure is simple and the number of the available process variables for the control structure configuration is limited. Hence the counting of the actual DOF is done based on the following preconditions which assume a tightly controlled C3 pre-cooler module [25].

- The LNG throughput rate is directly controlled by the LNG V/V.
- The pre-cooler keeps constant initial temperatures of the NG feed and the CMR loop.
- The streams passing through the intercooler and the aftercooler modules in the compressor cycle are kept at 30 °C.
- The compressor systems include the anti-surge control scheme.

Above assumptions eliminate variables 5-9. Then the remaining MVs are the LNG flow rate controlled by LNG V/V, the flow rates of the cold mixed refrigerant liquid (CMRL) and the cold mixed refrigerant vapor (CMRV), respectively, and the CMR compressor speed (C Speed). Among these, the LNG flow rate is selected as the measured disturbance. Then the possible candidates of MVs for the CMR loop in the C3MR process are CMRL and CMRV and C Speed.

A recommended selection of the CVs, also according to the reference study [25], is the temperature (LNG T) of the LNG product stream since LNG T affects both the composition and the throughput of LNG. Besides LNG T, the temperature difference of

Table 2. Operating parameters of the C3MR process units in Fig. 2

CMR 1st stage compressor		CMR separator	
Description [Unit]	Value	Description [Unit]	Value
Speed [rpm]	3531	Vessel volume [m³]	200
Actual volume flow rate [m³/h]	86250	Operating temperature [°C]	−33.15
Head [m]	17680	Operating pressure [barA]	49.07
Efficiency [%]	82		
CMR 2nd stage compressor		**Control valves**	
Description [Unit]	Value	Description	C_V
Speed [rpm]	3531	CMRV JT valve	75
Actual volume flow rate [m³/h]	15180	CMRL JT valve	177.5
Head [m]	6302	LNG V/V valve	265.6
Efficiency [%]	83		

Table 3. Suggested MVs and CVs for the DMC configuration with pairing descriptions

Variables		Description
MV	CMRL OP (CMRL flow rate)	CMRL JT valve opening
	CMRV OP (CMRV flow rate)	CMRV JT valve opening
	C Speed	Compressor speed
CV	LNG T	LNG temperature
	dT of HEX	Temperature difference of CMR and CMRV in Liquefier

between the CMR outlet and CMRV inlet in the liquefier (dT of HEX) can be selected as an auxiliary CV among the several candidates of potentially self-optimizing variables to control the energy efficiency. Drawing a steady-state optimality map of a given liquefaction process is a good way to evaluate the relationships between the compressor duty and other process variables by studying their stable operational trajectories [34]. In the reference study, the fixed value of dT of HEX produces the most similar trajectory to the optimal compressor duty curve drawn on the steady-state optimality map of the C3MR process. It is shown on the optimality map that by controlling dT of HEX, the compressor duty curve does not violate the infeasible region limited by the dew point of the CMR stream that enters the condensing cycle. Thus dT of HEX can be utilized as a CV that is indirectly related to the energy efficiency of the compressors. Summing these up, the control structure of the DMC is configured to have three MVs and two CVs in total. This list of MVs and CVs is summarized in Table 3, and it is shown that the flow rate of a given CMR stream is regulated by the opening of the corresponding actuator valve.

2. Interaction Analysis

Although the reference study in [25] excluded the C speed from the suggested MV candidate by assigning a fixed value, our example adds one more DOF to the system control by including it as a possible MV. One of the aims of this study is to show that it is possible to control the CMR loop more efficiently if the C Speed is included among the MVs, since it is directly related to the compressor power usage and the CMR flow rate. Step input tests and steady-state RGA analyses are conducted for all one-on-one combinations of MVs and CVs to understand how strong the interactions between MVs and CVs are. The RGA analysis of the Aspen HYSYS Dynamics model given in Table 4 demonstrates that the C Speed has a certain influence over LNG T and dT of HEX and supports the argument that it is appropriate to include the C Speed as a possible MV. The results of the RGA analysis are calculated as scaled values in percentages which are normalized with respect to their allowed ranges [35].

Table 4 also illustrates the necessity of a MIMO control algorithm on the C3MR process. Note that while dT of HEX primarily interacts with CMRL OP and secondly with C Speed, LNG T can be mainly controlled by changes on both CMRV OP and C Speed. Hence Table 4 supports the argument that for the given C3MR process, the use of the multivariable optimal control such as the DMC could result in a more efficient control than the PI or PID algorithm since it takes account of interactions among multiple process variables while predicting process outputs.

Table 4. Steady-state RGA analysis of the C3MR process based on Table 3

Variables	CMRL OP	CMRV OP	C Speed
LNG T	0.1826	0.3464	0.4710
dT of HEX	0.8170	0.0539	0.1291

3. Controller Setups

To support the result of the steady-state RGA analysis in Table 4 that indicates the necessity of a multivariable optimal controller on the C3MR process, we test the efficiency of the DMC algorithm by comparing its control result with those from two PI control setups, which are defined as Case A and Case B. The two PI control loops differ by whether the C Speed is among the MVs or not. Case A is a two-by-two PI controller with CMRV OP - LNG T and CMRL OP - dT of HEX control loops, whereas case B is a three-by-three PI controller in which the C Speed - Compressor suction pressure control loop is added on the existing control loops in Case A. According to the RGA analysis in Table 4, the C Speed should be controlling the LNT Temp since its relative gain is nearer to one than that of the CMRV OP. However, the prerequisite of this study is that the compressors should operate in a stable condition, not overrunning the compressor surge lines. Thus, Case A and Case B are adjusted so that the CMRV OP controls the LNG T and the C Speed is manipulated to maintain a constant CMR pressure in the CMR compression loop to reduce instabilities in the compressor units which might occur during the dynamic simulations. All the configurations of the DMC module and the two PI control modules are separately illustrated in Fig. 3 and Fig. 4.

The DMC in MATLAB 2014a environment calculates and transmits the current input signals directly to the valve openings and compressor units in Aspen HYSYS. This transfer of process information between MATLAB and Aspen HYSYS spreadsheet is exe-

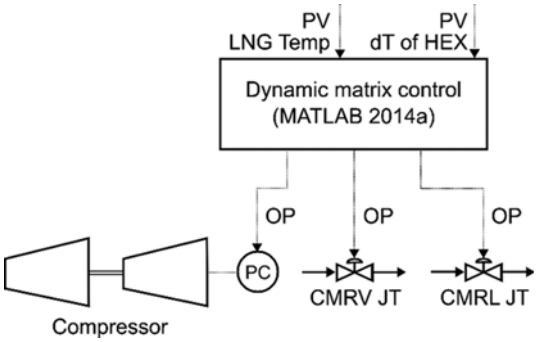

Fig. 3. Multivariable DMC scheme applied on the C3MR process.

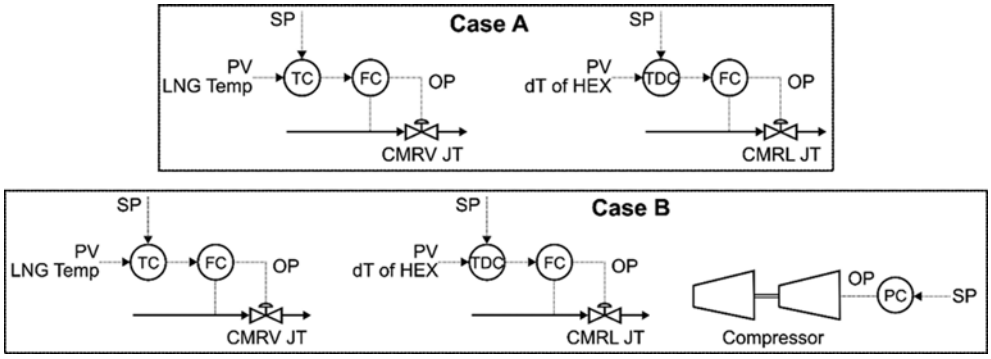

Fig. 4. Two-by-two PI controller (Case A) and three-by-three PI controller (Case B) schemes applied on the C3MR process.

cuted with a process changing rate of 5%/s via HYSYSlib function developed by Berglihn [36]. All of the PI controllers excluding the C Speed controller operate in a two-step cascade control procedure on Aspen HYSYS environment so that the slave (secondary) controllers calculate the current inputs using the setpoint errors provided by the master (primary) controllers [37]. Cascade control loops can effectively limit the propagation of disturbance effects throughout the entire process by enhancing the control response speed with a fast-responding slave control loop. This is a widely accepted approach in LNG processing plants having multiple sensors measuring different variables such as the stream temperatures and the flow rates [24,25]. Although the derivative control action could be added in the master control loop of the cascade control [37], it is excluded for this case study to simplify the controller tuning process. This is because the C3MR process has multiple parallel cascade control loops having up to five feedback controllers which need to be tuned simultaneously. One additional control parameter, the derivative time constant not only significantly raises the difficulty of tuning for the already complex control system, but also potentially requires an additional design of a low-pass filter to reduce response sensitivity of disturbances [38,39].

DMC SIMULATION

1. System Identification

The DMC algorithm can utilize step response coefficient matrices as the model information when definite dynamic model equations are not available. The step response coefficient matrix is obtained by the system identification when several different step input responses are fitted into an empirical transfer function model. Fig. 5 shows the results of the step response tests from the Aspen HYSYS dynamic model in Fig. 2. The data sequences from this simulation are used to fit a transfer function matrix through MATLAB using the 'tfest' function. The result is shown in Eq. (6), where u_1: CMRL OP; u_2: CMRV OP; u_3: C Speed; y_1: LNT T and y_2: dT of HEX.

$$\begin{bmatrix} y_1 \\ y_2 \end{bmatrix} = \begin{bmatrix} \dfrac{-0.0007398s - 2.434e^{-8}}{s^2 + 0.0009556s + 3.271e^{-8}} & \dfrac{-0.004784s + 6.799e^{-9}}{s^2 + 0.01373s + 4.649e^{-18}} \\ \dfrac{0.05515s + 1.238e^{-4}}{s^2 + 0.02176s + 2.64e^{-5}} & \dfrac{0.01819s - 6.542e^{-4}}{s^2 + 0.1499s + 0.003292} \\ \dfrac{-0.006581s - 1.754e^{-5}}{s^2 + 0.03835s + 3.92e^{-5}} & \\ \dfrac{-0.02555s - 2.882e^{-5}}{s^2 + 0.036s + 6.439e^{-5}} & \end{bmatrix} \begin{bmatrix} u_1 \\ u_2 \\ u_3 \end{bmatrix} \quad (6)$$

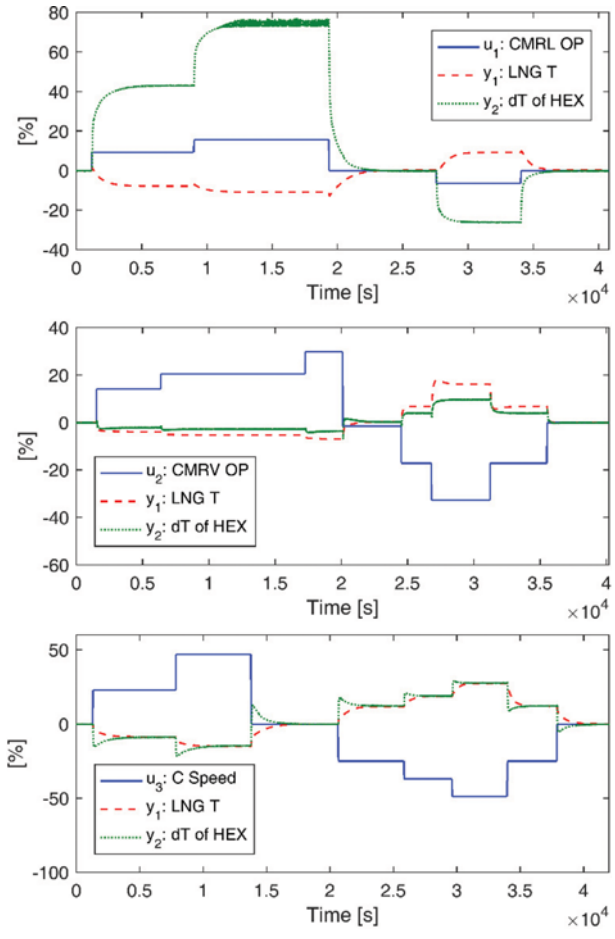

Fig. 5. Dynamic step responses of the C3MR process (top: step response of CMRL OP, middle: step response of CMRV OP, bottom: step response of C speed).

The normalized root-mean-square error (NRMSE) fitnesses of the transfer functions in Eq. (6) and the original Aspen HYSYS dynamic

Table 5. NRMSE fitness of the transfer functions in Eq. (6) obtained from the Aspen HYSYS dynamic model of the C3MR process

CV	MV		
	u_1: CMRL OP	u_2: CMRV OP	u_3: C Speed
y_1: LNG T	75.59%	76.82%	76.62%
y_2: dT of HEX	95.60%	65.10%	77.55%

PFD are shown in Table 5 which are calculated using the 'compare' function in MATLAB.

$$\text{fitness} = 100\% \times \left(1 - \frac{|\hat{y} - y|}{|\hat{y} - \text{mean}(\hat{y})|}\right) \tag{7}$$

Based on these values calculated using Eq. (7) where $\hat{y}$ is the PFD data and y is the transfer function output, we may conclude that Eq. (6) depicts the general dynamics of the C3MR process with an acceptable accuracy. Consequently, a step response coefficient matrix is obtained from Eq. (6) also by MATLAB using the 'tfd2step' function.

2. DMC Application

The DMC module is formulated by using the step response coefficient matrix obtained in the previous section. In the DMC module, a quadratic objective function that is the sum of output measurement errors and input changes over a finite prediction horizon is minimized to result in an optimal future input sequence. This optimization step is repeated at each time step and lets the initial element of the newly calculated input sequence update the process feedback error. The steps of constructing the mentioned quadratic objective function are shown below; for an input vector $u(k) \in R^{n_u}$ and an output vector $y(k) \in R^{n_y}$, a step response coefficient matrix $S_k \in R^{n_y \times n_u}$ is defined for the time step k as follows;

$$S_k = \begin{bmatrix} S_{1,1,k} & S_{1,2,k} & \cdots & S_{1,n_u,k} \\ S_{2,1,k} & S_{2,2,k} & \cdots & S_{2,n_u,k} \\ \vdots & \vdots & \ddots & \vdots \\ S_{n_y,1,k} & S_{n_y,2,k} & \cdots & S_{n_y,n_u,k} \end{bmatrix}, \quad \forall k = 1, \cdots, n \tag{8}$$

k=n is the time when the process reaches a steady state with $S_n = S_{n+1} = \cdots = S_\infty$. Hence the first n time steps of the state vectors are sufficient to capture the total dynamic process change. Then y(k) is augmented for n time steps to form a new state vector $Y(k) \in R^{n \times n_y}$ shown in Eq. (9) and Eq. (10), where it is updated at each k by a new input change $\Delta u(k-1)$.

$$Y(k) = [y(k)^T \quad y(k+1)^T \quad \cdots \quad y(k+n-1)^T]^T \tag{9}$$

$$Y(k) = MY(k-1) + S\Delta u(k-1) \tag{10}$$

$$\Delta u(k) = u(k) - u(k-1) \tag{11}$$

$$M = \begin{bmatrix} 0 & I_y & 0 & \cdots & 0 & 0 \\ 0 & 0 & I_y & \ddots & 0 & 0 \\ \vdots & \vdots & \vdots & \ddots & \ddots & \vdots \\ 0 & 0 & 0 & \ddots & I_y & 0 \\ 0 & 0 & 0 & \ddots & 0 & I_y \\ 0 & 0 & 0 & \cdots & 0 & I_y \end{bmatrix}, \quad S = \begin{bmatrix} S_1 \\ S_2 \\ \vdots \\ S_{n-1} \\ S_n \end{bmatrix} \tag{12}$$

Secondly, a new vector $\hat{Y}(k+1|k)$ that predicts the future outputs for a prediction horizon p is calculated by using the future inputs $\Delta U(k)$ for a control horizon m with the addition of measurement errors. For the prediction, we assume there is no modeled disturbance present in the process.

$$\hat{Y}(k+1|k) = M_Y Y(k) + S_U \Delta U(k) + I_Y [y_m(k) - y(k)], \; m \le p \le n \tag{13}$$

$$\hat{Y}(k|k) = [y(k|k)^T \; \hat{y}(k+1|k)^T \; \cdots \; \hat{y}(k+p-1|k)^T]^T \tag{14}$$

$$\Delta U(k) = [\Delta u(k)^T \; \Delta u(k+1)^T \; \cdots \; \Delta u(k+m-1)^T]^T \tag{15}$$

$$M_Y = \begin{bmatrix} 0 & I_y & 0 & \cdots & \cdots & \cdots & \cdots & 0 \\ 0 & 0 & I_y & 0 & \ddots & \ddots & \ddots & \vdots \\ \vdots & \vdots & \vdots & \ddots & \ddots & \ddots & \ddots & 0 \\ 0 & 0 & 0 & \cdots & I_y & 0 & \cdots & 0 \end{bmatrix}, \quad S_U = \begin{bmatrix} S_1 & 0 & \cdots & \cdots & 0 \\ S_2 & S_1 & 0 & \cdots & 0 \\ \vdots & \vdots & \ddots & \ddots & \vdots \\ S_m & S_{m-1} & \cdots & \cdots & S_1 \\ \vdots & \vdots & \ddots & \ddots & \vdots \\ S_p & S_{p-1} & \cdots & \cdots & S_{p-(m-1)} \end{bmatrix} \tag{16}$$

$$I_Y = [I_y \; I_y \; \cdots \; I_y]^T$$

In the final step, $\hat{Y}(k+1|k)$ is inserted in the objective function J that is minimized in the optimization problem in Eq. (17) to produce an optimal sequence $\Delta U(k)$.

$$J = \min_{\Delta U(k)} [|\Gamma^Y \{\hat{Y}(k+1|k) - R(k+1|k)\}|^2 + |\Gamma^U \Delta U(k)|^2] \tag{17}$$

$$u_{min} \le u(k+j) \le u_{max}$$

$$\Delta u(k+j) \le \Delta u_{max}$$

$$y_{min} \le y(k+j) \le y_{max}, \quad \forall j \ge 0$$

The overall steps repeat themselves when the first value in the resulting $\Delta U(k)$ vector is used as the new input change $\Delta u(k)$ that updates the new Y(k+1) [15-17,40,41].

SIMULATION RESULTS

The simulation result in which the DMC algorithm is applied on the C3MR process is compared with the simulation results in which the two-by-two (Case A) and three-by-three (Case B) cascade PI controllers are adopted. The PI controllers are tuned by the relay-based tuning method, which is an embedded function in Aspen HYSYS. The control parameters of the DMC and the PI

Table 6. Control parameters of DMC

Parameters	Values
u_{min}	$[-10 \; -35 \; -50]^T$
u_{max}	$[16 \; 30 \; 50]^T$
Δu_{max}	$[6 \; 8 \; 10]^T$
p	100
m	20
$(\Gamma^Y)^2$	diag(20, 1)
$(\Gamma^U)^2$	diag(80, 50, 20)

Table 7. Control parameters of PI controllers

Controller description	K_C	τ_I [min]
LNG Temp controller (Master)[a]	3.48	0.624
dT of HEX controller (Master)[b]	0.0961	0.312
CMRL flow rate controller (Slave)[a]	0.139	0.00671
CMRV flow rate controller (Slave)[b]	0.36	0.00577
C speed controller	2.8	0.0204

controllers are shown in Table 6 and Table 7, respectively. Note that the master and the slave controllers in the cascade control loops are paired with the same superscript in the controller description in Table 7.

We consider two examples for the analysis of the controller efficiency. The following unmeasured disturbances are added to the dynamic process simulation in the direction of increasing the load of the liquefaction energy; the first scenario is a 3% step input on the NG flow rate and the second scenario is a −1 barA step decrease in the NG injection pressure. The results of the dynamic simulations for each scenario of the unmeasured disturbance are illustrated in Fig. 6, Fig. 7 and Table 8. The noise present on the process output sequence in the DMC example could be attributed to the time lapse during the transferring information between Aspen HYSYS and MATLAB at each time step. In both scenarios, the dynamic simulations using the DMC show better efficiency of han-

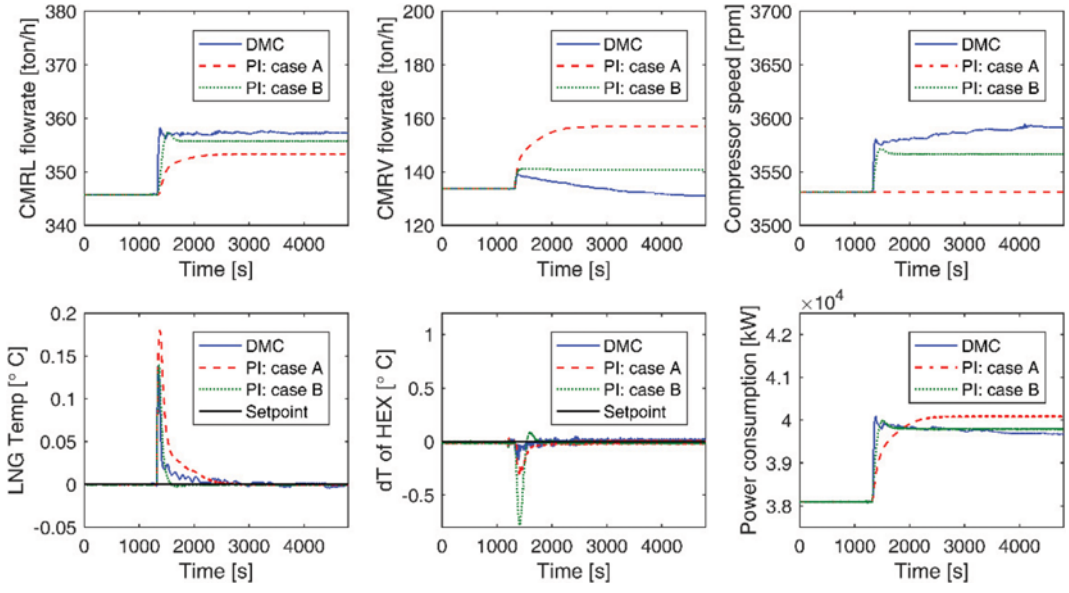

Fig. 6. Dynamic simulation results of the DMC and the PI controllers (Case A, Case B) for a 3% step input addition to NG injection flow rate.

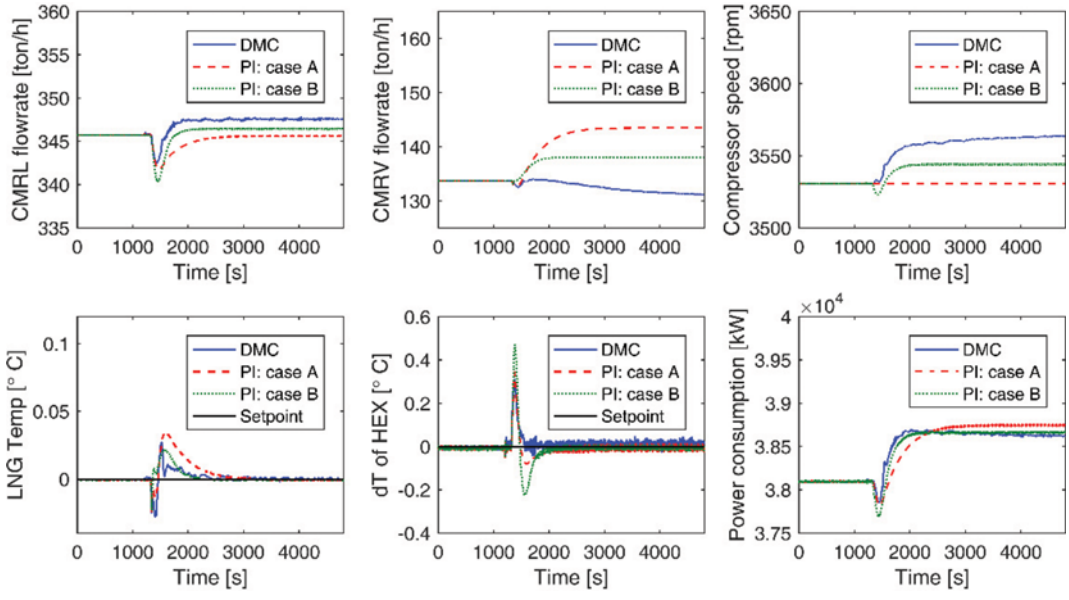

Fig. 7. Dynamic simulation results of the DMC and the PI controllers (Case A, Case B) for a -1barA step decrease of NG injection pressure.

Table 8. Comparison between the dynamic simulation results of the DMC and the PI controllers (Case A, Case B)

Scenario	Process variable	DMC	PI control (case A)	PI control (case B)
NG flow rate: +3%	CMRL flow rate [ton/h]	357.36	353.30	355.72
	CMRV flow rate [ton/h]	131.12	157.00	140.90
	Total CMR flow rate [ton/h]	488.483	510.22	496.62
	Power consumption [kW]	39673	40083	39798
	Power consumption difference [kW]	0	+411	+125
NG injection pressure: −1 barA	CMRL flow rate [ton/h]	347.61	345.63	346.46
	CMRV flow rate [ton/h]	131.20	143.51	138.07
	Total CMR flow rate [ton/h]	478.81	489.14	484.53
	Power consumption [kW]	38621	38742	38661
	Power consumption difference [kW]	0	+121	+40

dling the increased load of cooling duty with more robust control input sequences compared to the PI controller counterparts.

1. Increasing NG Injection Flow Rate

As the liquefaction load is increased by the unmeasured disturbance, the amount of power consumption naturally is increased in all three control cases, with the DMC using the least amount of power. According to Fig. 6, the PI controller in Case A has a fixed C Speed and hence raises the flow rates of both CMRL and CMRV to handle the extra required cooling duty. The PI controller in Case B increases all of the MVs including the flow rates of CMRL and CMRV and the C Speed. It saves more power than Case A, slightly less than the DMC, as it utilizes C Speed as one of the MVs. However, the instability of Case B on the output variables is considerably larger than that from the DMC, especially on the dT of HEX. The DMC increases both the CMRL flow rate and the C Speed but reduces the CMRV flow rate, unlike the PI controllers. The reason why the DMC alone reduces the CMRV flow rate is because the discharge pressure of the compressor rises when the C Speed is increased. Then the ratio of CMRL rises also, whereas the CMRV flow rate is decreased. Although the total amount of the CMR flow rate is decreased by the DMC due to the lesser CMRV flow rate, the MCHE is now able to handle a larger amount of cooling duty than before, since the CMRL has higher specific heat than the CMRV. Reduced power consumption is thought to result from the decrease in the total amount of the CMR flow rate, reducing the overall amount of work added to the compressor despite the increased C Speed.

2. Decreasing the NG Injection Pressure

At a constant temperature, the enthalpy of the NG stream is increased when the injection pressure of the NG feed is reduced by an external disturbance, which also forces larger cooling duty on the C3MR process. However, pressure decrease of −1 barA has relatively small effect on the system compared to the NG flow rate increase in the first scenario. Therefore, the magnitudes of the process response to the disturbances are smaller, although the general tendencies of the dynamic sequences of the C3MR process are similar in both Fig. 6 and Fig. 7. Hence we may conclude that the DMC produces not only the control input sequences that are more robust and optimal but also uses less amount of power than the PI controllers by taking the interactions between the process variables into account.

CONCLUSION

We analyzed the effectiveness of a multivariable optimal control algorithm on the C3MR process by comparing the dynamic simulation including a DMC module with two counter-examples with different structures of cascade PI controllers. A dynamic model of the C3MR process developed on Aspen HYSYS 7.3 was combined with the DMC built on MATLAB 2014a using the rigorous step response coefficient matrix produced by the dynamic process simulation. Each control structure was analyzed by its ability on how robust it responds to the two scenarios with unmeasured disturbances increasing the cooling duty and also by its influence on the process efficiency. Based on the RGA analysis, we have expanded the range of the possible MVs to include the C Speed, which has been avoided by the previous researchers. The dynamic simulation shows that it is capable of enhancing the process efficiency when manipulated within the safety margin not overrunning the compressor surge line. In conclusion, the DMC application demonstrates that it is capable of considering the multivariable interaction during the process regulation, unlike the other PI controllers. Also, its control actions generally undergo less overshooting, possibly with the help of the prediction algorithm of the future process variables and the addition of the process variable constraints.

ACKNOWLEDGEMENTS

This research was supported by Development of Sensor-based Virtual Plant Engineering Technology for the Support of Plant O&M project (10048341) funded by the Ministry of Trade, Industry & Energy of South Korea.

NOMENCLATURE

H : stream enthalpy
I_y : identity matrix with dimension of y
P : stream pressure
P_c : critical pressure
R : gas constant
$R^{i\times j}$: set of real numbers with a dimension of i×j
S : stream entropy
S_k : step response coefficient matrix at k^{th} time step

T : stream temperature
T_c : critical temperature
ΔU : optimized augmented vector of Δu for m time steps starting from t=k
V_m : stream molar volume
Y : augmented vector of y for n time steps starting from t=k
Z : compressibility factor
Γ^U : weighting factor of ΔU
Γ^Y : weighting factor of Y
k : order of the time step
m : control horizon
n_u : dimension of u
n_y : dimension of y
p : prediction horizon
s : frequency variable
$s_{i,j,k}$: step response coefficient of u_j and y_i at t=k
t : time
Δt : length of a time step
u : input vector
u_i : i^{th} input variable
Δu : change in u
y : output vector
y_i : i^{th} output variable
$\hat{y}$ (k+i|k) : estimated output value at t=k+i based on y(k)
ω : acentric factor

REFERENCES

1. S. Azzarello, *Energy price spread: Natural gas vs. crude oil in the US*, Market Insights, CME Group (2014).
2. V. Smil, *Natural gas: fuel for the 21st century*, West Sussex: John Wiley & Sons, Inc. (2015).
3. D. Burns, J. McLinn and M. Porter, *Navigating Oil Price Volatility*, Chemical Engineering Progress (CEP), AIChE (2016).
4. S. Mokhatab, J. Y. Mak, J. V. Valappil and D. A. Wood, *Handbook of Liquefied Natural Gas*, Gulf Professional Publishing (2014).
5. Q. Wang and R. Li, *Renewable and Sustainable Energy Reviews*, **54**, 925 (2016).
6. ExxonMobil, *The outlook for energy: a view to 2040* (2013).
7. ExxonMobil, *The outlook for energy: a view to 2040* (2015).
8. J. Hwang and K.-Y. Lee, *Comput. Chem. Eng.*, **63**, 1 (2014).
9. F. Faber and L. R. Resweber, *Floating LNG solutions from the drawing board to reality*, Offshore Technology Conference, Houston, Texas (2002).
10. D. Wood, S. Mokhatab and M. J. Economides, *Offshore natural gas liquefaction process and development issues*, SPE Annual Technology Conference and Exhibition, Anaheim, California (2007).
11. W. H. Zhao, J. M. Yang, Z. Q. Hu and Y. F. Wei, *Ocean Eng.*, **38**, 14 (2011).
12. S. Lee, N. V. D. Long and M. Lee, *Ind. Eng. Chem. Res.*, **51**, 30 (2012).
13. W. Won, S. K. Lee, K. Choi and Y. Kwon, *Korean J. Chem. Eng.*, **31**, 5 (2014).
14. Y. A. Husnil, G. Yeo and M. Lee, *Chem. Eng. Res. Design*, **92**, 4 (2014).
15. D. M. Prett, B. L. Ramaker and C. R. Cutler, US Patent, 4,349,869 (1982).
16. C. E. Garcia and A. M. Morshedi, *Chem. Eng. Commun.*, **46**, 73 (1986).
17. C. E. Garcia, D. M. Prett and M. Morari, *Automatica*, **25**, 3 (1989).
18. W. A. Poe and S. Mokhatab, *Hydrocarbon Processing*, **86**, 6 (2007).
19. W. Sturm, M. Parra-Calvache, F. Chantant and J. van Opstal *Unlocking the potential of modern control and optimization strategies in LNG production*, 1st Annual Gas Processing Symposium (2009).
20. B. Foss, *Control Eng. Practice*, **20**, 10 (2012).
21. S. Mokhatab and W. A. Poe, *Handbook of Natural Gas Transmission and Processing*, Second Ed., Gulf Professional Publishing (2012).
22. K. den Bakker, *A step change in LNG operations through advanced process control*, *23rd World Gas Conference*, Amsterdam (2006).
23. H. J. Kim, C. C. Park, J. Y. Lee C. S. Lee and M. H. Kim, *J. Mechanical Sci. Technol.*, **30**, 4 (2016).
24. J. A. Mandler, P. A. Brochu and J. R. Hamilton, US Patent, 5,791,160 (1998).
25. Y. A. Husnil and M. Lee, *AIChE J.*, **60**, 7 (2014).
26. D. Helgestad, *Modelling and optimization of the C3MR process for liquefaction of natural gas*, Norwegian University of Science and Technology, NTNU (2009).
27. A. Alabdulkarem, A. Mortazavi, Y. Hwang, R. Radermacher and P. Rogers, *Appl. Therm. Eng.*, **31**, 6 (2011).
28. D. B. Robinson, D.-Y. Peng and S. Y. Chung, *Fluid Phase Equilib.*, **24**, 1 (1985).
29. J. de Hemptinne and P. Ungerer, *Fluid Phase Equilib.*, **106**, 1 (1995).
30. C. Li, W. Jia and X. Wu, *Application of Lee-Kesler equation of state to calculating compressibility factors of high pressure condensate gas*, Energy Procedia **14** (2012).
31. Y. V. C. Rao, *Chemical Engineering Thermodynamics*, Universities Press (1997).
32. Aspen Technology, Inc., *Aspen physical property system: Physical property methods V7.3* (2011).
33. J. B. Jensen and S. Skogestad, *Ind. Eng. Chem. Res.*, **48**, 14 (2009).
34. Y. A. Husnil and M. Lee, *J. Chem. Eng. Jpn.*, **47**, 8 (2014).
35. J. D. Perkins, *Interactions between process design and process control*, Pergamon Press (1992).
36. M. J. Bland, *Optimisation of an ammonia synthesis loop*, Norwegian University of Science and Technology, NTNU (2015).
37. D. E. Seborg, T. F. Edgar, D. A. Mellichamp and F. J. Doyle III, *Process Dynamics and Control*, 3rd Ed., Wiley (2010).
38. K. H. Ang, G. Chong and Y. Li, *IEEE Trans. Control Syst. Technol.*, **13**, 4 (2005).
39. A. Visioli, *Practical PID Control*, Springer (2006).
40. P. Lundström, J. H. Lee, M. Morari and S. Skogestad, *Comput. Chem. Eng.*, **19**, 4 (1995).
41. A. M. Morshedi, C. R. Cutler and T. A. Skrovanek, *Optimal solution of dynamic matrix control with linear programming techniques (LDMC)*, American Control Conferences (IEEE) (1985).

APPENDIX

The performance curves of two compressors positioned in the CMR loop in the C3MR process are illustrated in Fig. 8 and Fig. 9, respectively. These data are obtained by the steady-state simulation in Aspen HYSYS 7.3.

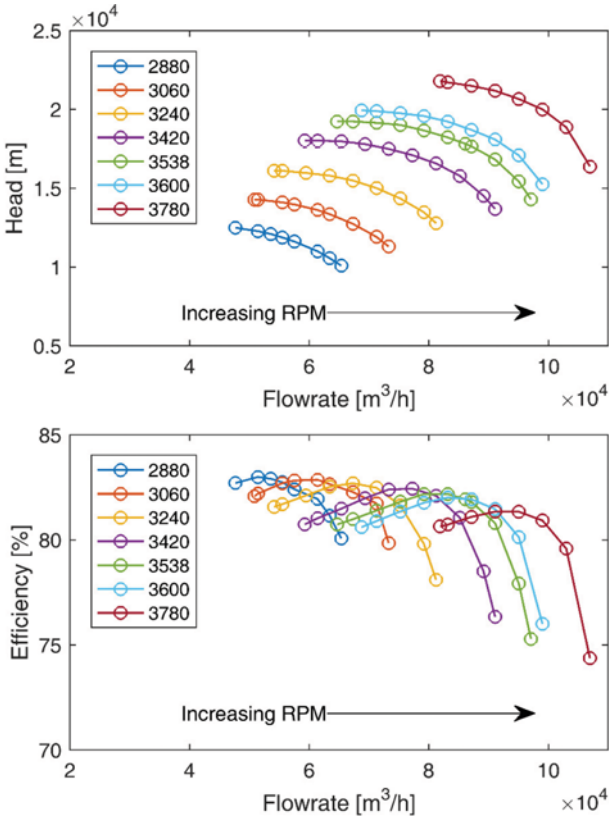

Fig. 8. Performance curves of the first compressor in the CMR loop (top: compressor head, bottom: compressor efficiency).

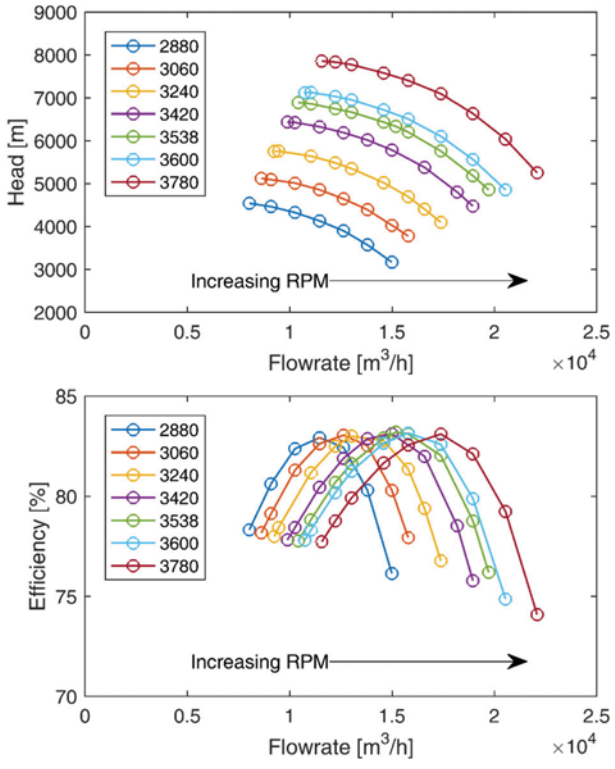

Fig. 9. Performance curves of the second compressor in the CMR loop (top: compressor head, bottom: compressor efficiency).